

Supporting Information for

Photocatalytic and photoelectric properties of cubic Ag₃PO₄ sub-microcrystals with sharp corners and edges

Yingpu Bi,^{*a,b} Hongyan Hu,^a Shuxin Ouyang,^b Gongxuan Lu,^{*a} Junyu Cao,^b and Jinhua Ye^{*b}

^a State Key Laboratory for Oxo Synthesis & Selective Oxidation, and National Engineering Research Center for Fine Petrochemical Intermediates, Lanzhou Institute of Chemical Physics, CAS, Lanzhou 730000, China.

^b International Center for Materials Nanoarchitectonics (MANA), and Research Unit for Environmental Remediation Materials, National Institute for Materials Science (NIMS), Tsukuba, 305-0047, Japan. E-mail: jinhua.ye@nims.go.jp

*To whom correspondence should be addressed.

Email: jinhua.ye@nims.go.jp; yingpubi@licp.ac.cn; gxl@lzb.ac.cn

Experimental Section

1. Synthesis of cubic Ag₃PO₄ crystals

The Ag₃PO₄ sub-microcubes were prepared by using silver-ammino complex as the silver ions source. In a typical synthesis, AgNO₃ (0.2 g) was solved in aqueous solution. Ammonia aqueous solution (0.1 M) was added with drop by drop to the above solution to form a transparent solution. Then, Na₂HPO₄ aqueous solution (0.15 M) was added, and olivine Ag₃PO₄ crystals with cubic structure have been synthesized.

2. Photocatalytic reactions

In all catalytic activity of experiments, the samples (0.2 g) were put into a solution of MB dye (100 ml, 8 mg/L), which was then irradiated with a 300W Xe arc lamp equipped with an ultraviolet cutoff filter to provide visible light with $\lambda \geq 420$ nm. The degradation of MB dye was monitored by UV/Vis spectroscopy (UV-2550, Shimadzu). Before the spectroscopy measurement, these photocatalysts were removed from the photocatalytic reaction systems by a dialyzer.

3. Photoelectric conversions

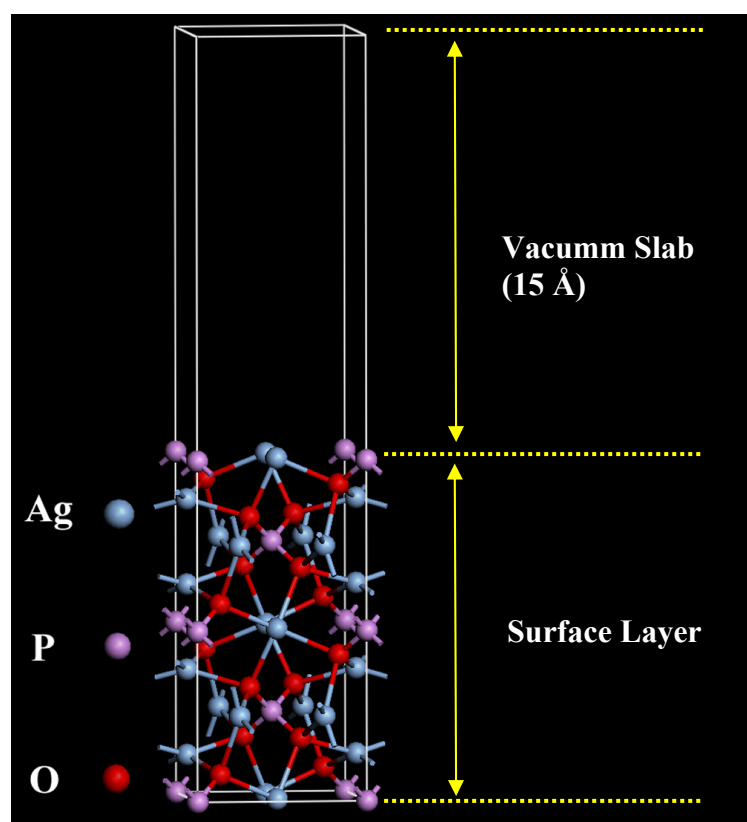
The photoelectric conversion properties were investigated in a conventional three-electrode cell by using computer-controlled electrochemical workstation (CHI 660D). 50 mg catalysts was suspended in 2 mL nafion aqueous solution (1 wt%), the mixtures were ultrasonically scattered for 15 min to form homogeneous solution. Then, 0.1 mL solution was dropped on the Fluorine doped tin oxide (FTO) glass (0.5×4 cm). After evaporation of the water in air, the catalyst was attached onto the surface of FTO glass. A Pt wire, saturated calomel electrode (SCE), and 0.1 M sodium sulfate were used as the working electrode, the counter-electrode, the reference electrode, and the electrolyte, respectively. The current-time (*i-t*) curves were collected at 1 V vs SCE. The light source was a 300W Xe lamp, and a cutoff filter of 420nm was employed for the visible-light irradiation.

4. Characterizations

SEM and FE-SEM images were taken using a field-emission scanning electron microscope (JSM-6701F, JEOL) operated at an accelerating voltage of 5 kV. An energy-dispersive (ED) detector was equipped with this field-emission scanning electron microscope and operated at an accelerating voltage of 15 kV. The X-ray diffraction spectra (XRD) measurements were performed on a Rigaku RINT-2000 instrument using Cu K α radiation (40 kv). The XRD patterns were recorded from 10° to 90° with a scanning rate of 0.067°/ s. UV/Vis absorption spectra were taken at room temperature on a UV-2550 (Shimadzu) spectrometer. The surface area of the sample was measured by the BET method (Shimadzu Gemini 2360, Micromeritics).

5. Calculations

Our electronic structure calculations were performed using a standard Cambridge serial total energy package (CASTEP) code¹ based on the density-functional theory (DFT). The surface model was constructed as the following figure, which consists of a surface layer of $1\times 1\times 2$ Ag_3PO_4 supercell and a 15 Å of vacuum slab. The two atomic layers of top and bottom were relaxed while the other atomic layers were fixed. Before electronic-structure calculation, the geometry optimization was performed to generate a stable surface. For electronic-structure calculation, the electron-core interaction was represented via ultrasoft pseudopotentials with a plane-wave basis cutoff energy of 300 eV. The valence configurations of the pseudopotentials are $4d^{10}5s^1$ for Ag, $2s^22p^4$ for O, and $3s^23p^3$ for P. The electronic exchange-correlation energy was treated within the framework of the local density approximation (LDA). The self-consistent field (SCF) tolerance was 2×10^{-6} eV/atom. The FFT grid of basis in the model was $30 \times 30 \times 135$. The k-point set of $3 \times 3 \times 1$ was used.



Reference

1. Segall, M. D.; Lindan, P. L. D.; Probert, M. J.; Pickard, C. J.; Hasnip, P. J.; Clark, S. J.; Payne, M. C. J. Phys.: Cond. Matt. 2002, 14, 2717–2743.

Additional Figures

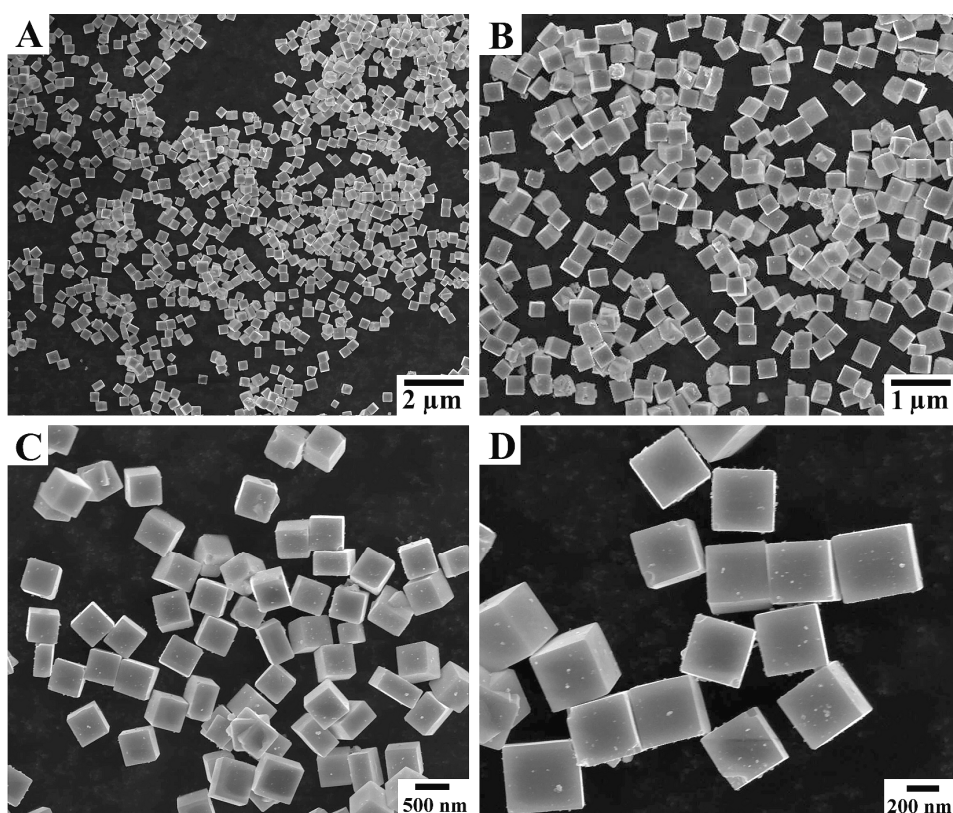


Fig. S1. (A-D) SEM images of cubic Ag_3PO_4 crystals with different magnifications.

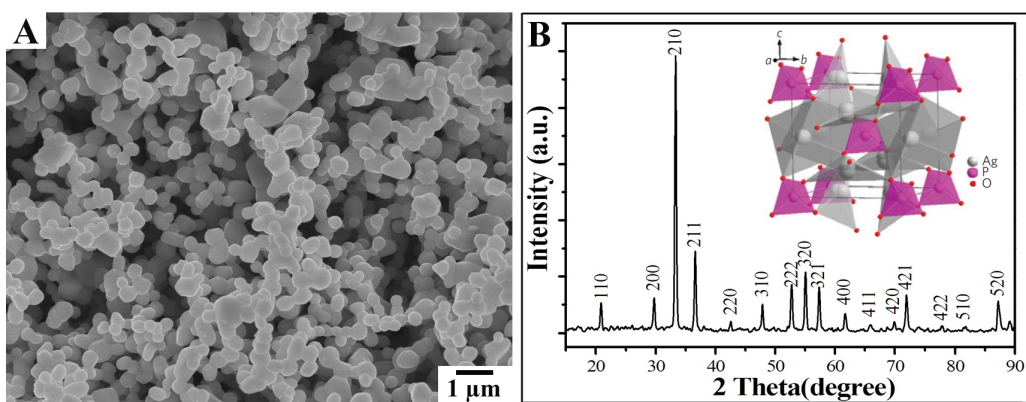


Fig. S2. (A) SEM images of irregular Ag_3PO_4 particles prepared by directly reacting AgNO_3 with Na_2HPO_4 , (B) XRD pattern of irregular Ag_3PO_4 particles.

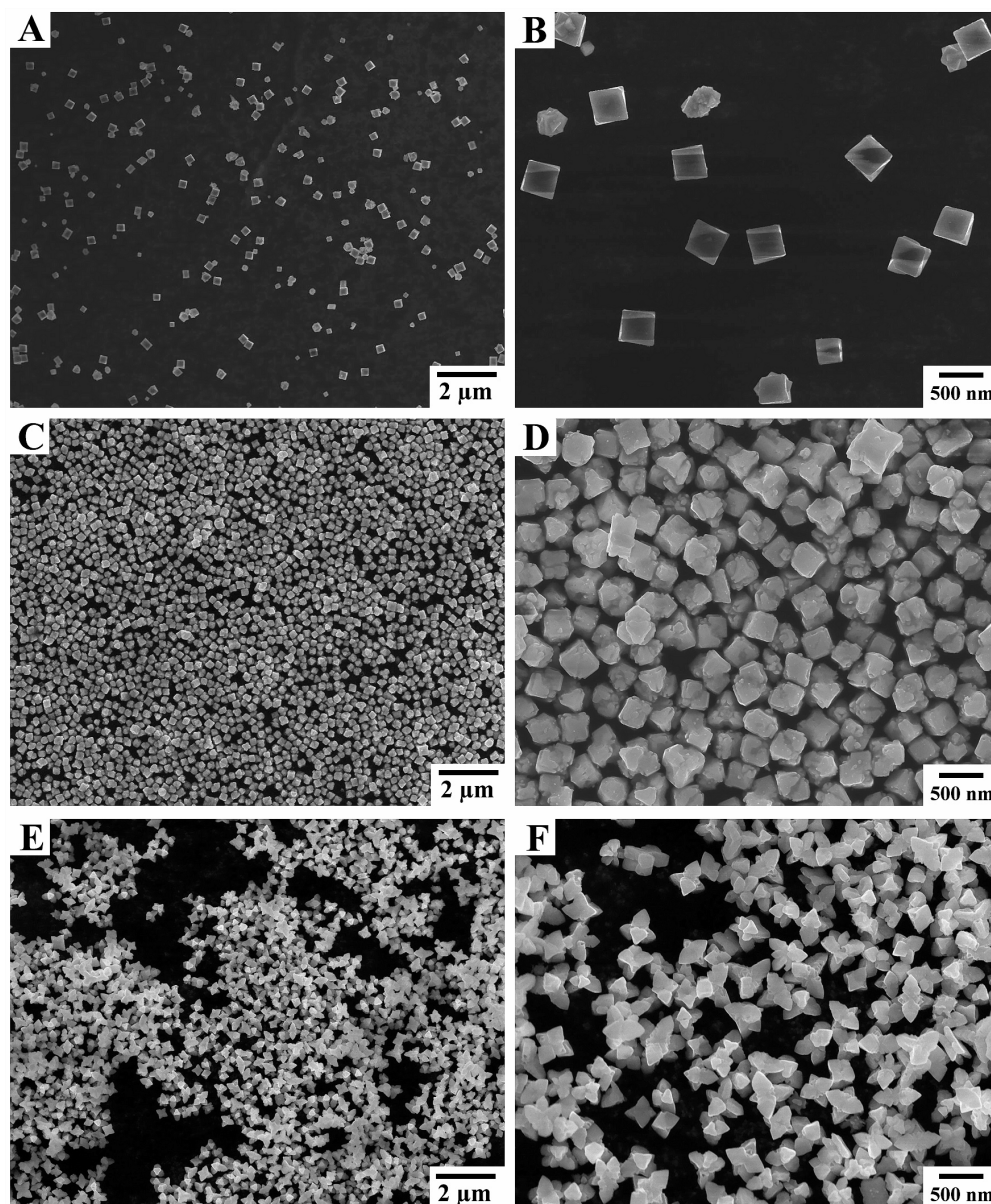
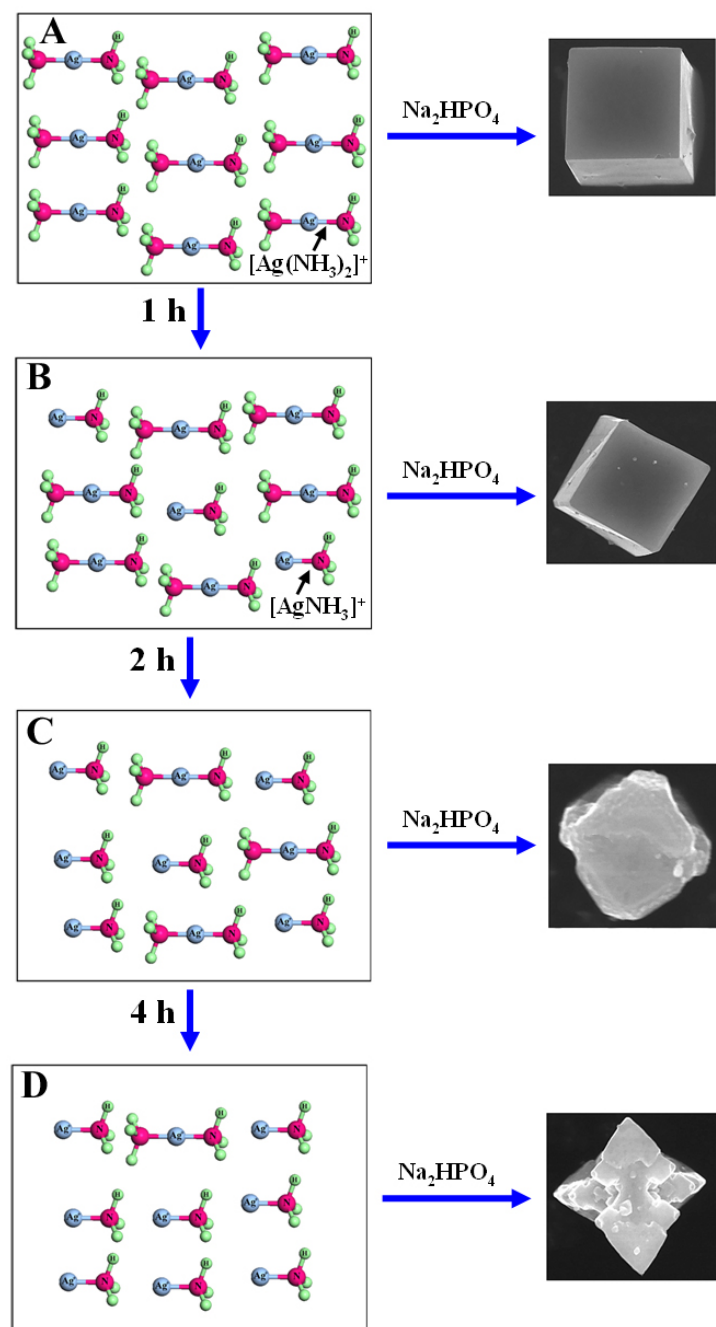


Fig. S3. Low and enlarged SEM images of Ag_3PO_4 products prepared with different aging time: (A,B) 1 h, (C,D) 2 h, (E,F) 4 h.



Scheme S1. Schematic illustration of the effects of the ratio variations between NH_3 and Ag in silver-ammonia complex on the morphologies of Ag_3PO_4 products with different aging time: (A) 0 h, (B) 1 h, (C) 2 h, (D) 4 H.

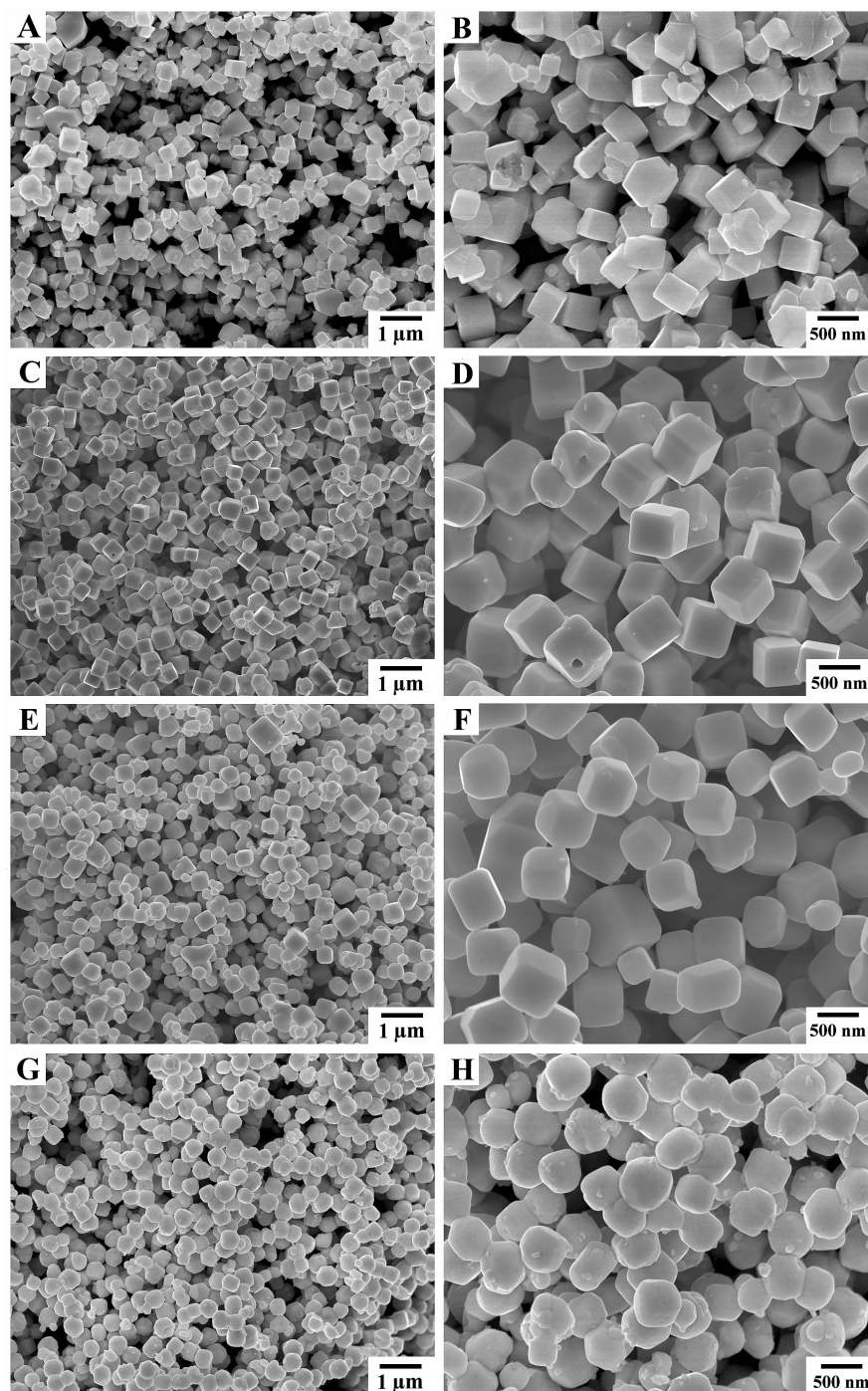


Fig. S4. Low and enlarged SEM images of Ag_3PO_4 products at different reaction temperatures: (A,B) 0 °C; (C,D) 40 °C; (E,F) 60 °C; (G,H) 80 °C.

Results and discussion

It should be noted that the synthetic temperature also play a important role in determining the morphologies and structures of the Ag_3PO_4 crystals. As shown in Fig. S4A,B, with decreasing the reaction temperature down to 0°C, the as-prepared Ag_3PO_4 cubes possess relatively poor uniformity and crystallinity. However, as shown in Fig. S4C,D, when the temperature has been increased up to 40°C, all the corners and edges of these Ag_3PO_4 cubes were slightly truncated, and the corresponding {110} planes emerged. With increasing the temperature to 40°C, the {110} planes of Ag_3PO_4 cubes transformed into curve structures, and the sharp corners and edges completely disappeared (shown in Fig. S4E,F). Furthermore, as shown in Fig. S4G,H, only irregular spherical Ag_3PO_4 particles have been formed in the obtained samples at the temperature of 80°C,. Accordingly, we consider that Ag_3PO_4 materials possess relatively high

solubility (0.02g/L, at 20°C), the solubility of Ag_3PO_4 has been increased by increasing the temperature. On the other hand, the corners and edges possess relatively high surface energies, which can be easily dissolved and cause the resultant products with non-perfect cubic structure or even spherical particles.

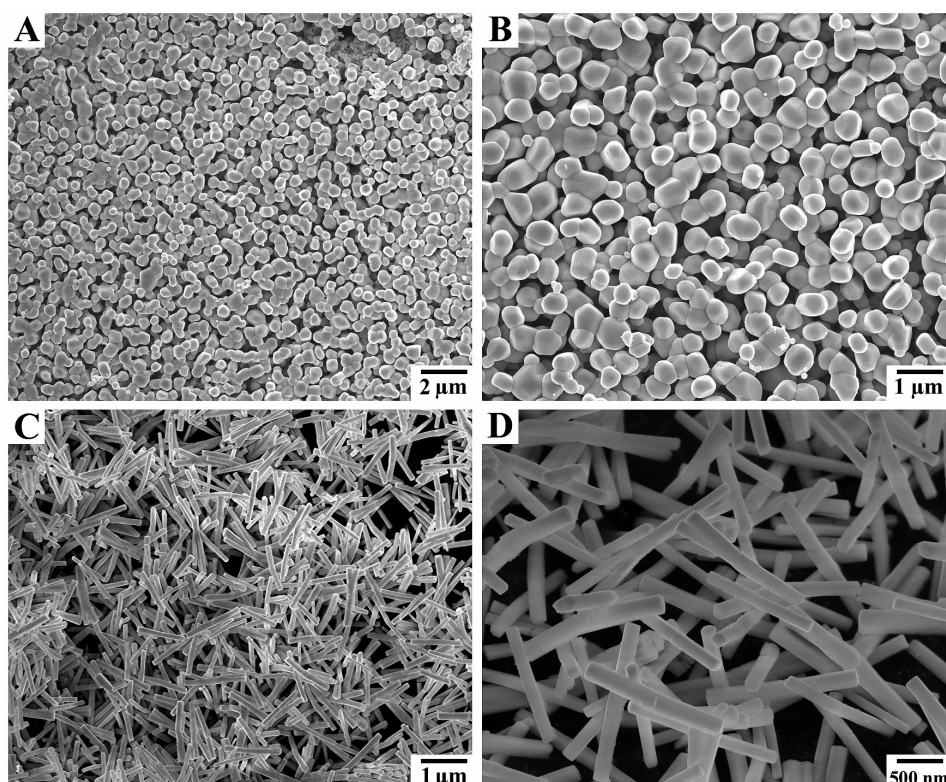


Fig. S5. (A, B) SEM images of AgBr products prepared by reacting $[\text{Ag}(\text{NH}_3)_2]^+$ with NaBr, (C, D) SEM images of Ag_2WO_4 products prepared by reacting $[\text{Ag}(\text{NH}_3)_2]^+$ with Na₂WO₄.

Results and discussion

Except the fabrication of Ag_3PO_4 cubes, this complex-precipitation strategy can also be used to prepare other semiconductor heterostructures. As shown in Figure S5A,B, when Na₂HPO₄ was replaced by NaBr to react with $[\text{Ag}(\text{NH}_3)_2]^+$ complex in this synthesis system, AgBr particles with flexuous nanostructures have been formed. Moreover, when Na₂WO₄ was used in this process, Ag_2WO_4 nanorods have been synthesized (shown in Figure S5C,D). More specifically, the generation rates of AgX (X= PO_4^{3-} , Br⁻, WO₄²⁻) were all strongly dependent on the $[\text{Ag}(\text{NH}_3)_2]^+$ complex precursor, which can be served as a general and facile synthesis process for the fabrication of semiconductor photocatalysts with novel morphology and structure.